

Random Access Protocol with Channel Oracle Enabled by a Reconfigurable Intelligent Surface

Victor Croisfelt, Fabio Saggese, Israel Leyva-Mayorga, Radosław Kotaba,
Gabriele Gradoni, and Petar Popovski

NOTE: This work has been submitted to the IEEE TWC for possible publication.

Copyright may be transferred without notice, after which this version may no longer be accessible.

Abstract

The widespread adoption of Reconfigurable Intelligent Surfaces (RISs) in future practical wireless systems is critically dependent on the design and implementation of efficient access protocols, an issue that has received less attention in the research literature. In this paper, we propose a grant-free random access (RA) protocol for a RIS-assisted wireless communication setting, where a massive number of users' equipment (UEs) try to access an access point (AP). The proposed protocol relies on a *channel oracle*, which enables the UEs to infer the best RIS configurations that provide opportunistic access to UEs. The inference is based on a model created during a training phase with a greatly reduced set of RIS configurations. Specifically, we consider a system whose operation is divided into three blocks: i) a downlink training block, which trains the model used by the oracle, ii) an uplink access block, where the oracle infers the best access slots, and iii) a downlink acknowledgment block, which provides feedback to the UEs that were successfully decoded by the AP during access. Numerical results show that the proper integration of the RIS into the protocol design is able to increase the expected end-to-end throughput by approximately 40% regarding the regular repetition slotted ALOHA protocol.

Index Terms

Reconfigurable intelligent surface (RIS), random access, channel oracle.

I. INTRODUCTION

RECONFIGURABLE Intelligent Surfaces (RISs) are low-power wireless system elements that can shape the radio waves to enable a smart radio environments [1], [2]. The majority of the literature on RIS-assisted communication systems has predominantly focused on the physical layer aspects, including the modeling of the related electromagnetic phenomena. This

includes recent work on physics-based derivation of channel models, that have extended plane wave expansions beyond the far-field approximation [3], as well as derived new expressions for the degrees of freedom of holographic MIMO communications [4]. On the one hand, many papers have shown potential benefits in terms of spectral and energy efficiencies of RIS-assisted systems in [5]; others have focused on the development of optimization methods for the RIS configuration alone or jointly with the access point (AP) precoding [6]–[8]. On the other hand, several works focus on the design and evaluation of channel estimation procedures in the presence of RIS [9]. A particular effort is made to reduce the overhead of the estimation procedure, which can be very high due to the high number of elements that composed the RIS [10]–[12]. However, less attention has been paid to protocol and control signaling aspects, which are crucial for system-level integration and operation of RIS.

An interesting first problem for integration of the RIS is to consider the massive machine-type communications (mMTC) scenario depicted in Fig. 1, where a massive number of users' equipment (UEs) or Internet-of-Things (IoT) devices communicate sporadically with the AP under the condition that the line-of-sight (LoS) towards the AP is phased. To improve the channel conditions and extend the coverage of the AP towards users with no LoS, a RIS is deployed in order to circumvent the phases and bring a low-energy consumption solution to the problem. In this version of the problem, the AP is assumed to be aware of the presence of the RIS with both entities being connected via an out-of-band control channel (CC) [5]. A new aspect of this scenario in comparison with the typical massive random access (RA) [13] is the additional need for the AP to control the RIS and use its capability of shaping the environment to improve the probability of access of the UEs. This requires the study of new RA protocols that consider the existence of the RIS on the environment to deal with IoT connectivity [14].

For RIS-assisted networks, there is a gap in the literature regarding the access procedure and related problems. The authors of [15] present designs for medium access control protocol that integrate RISs for multi-user communications. However, these works do not address the problem of access when channel state information (CSI) is unknown. In this regard, a closely related work is [16], where the authors consider the activity detection problem for unsourced RA by using the RIS to improve the channel quality and control channel sparsity; however, the work does not clarify how to adequately integrate it into the protocol design and how to use the RIS wave-shaping capabilities in a smarter way. In addition, the authors in [17] propose an activity detection algorithm that optimizes the phase shift configuration of the RIS to

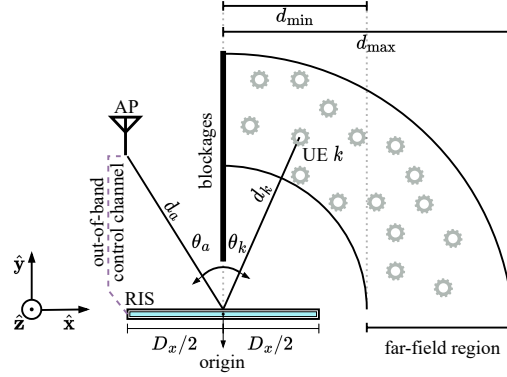


Fig. 1. Two-dimensional view of the massive RA setup assisted by a RIS of negligible thickness.

obtain optimal detection probability. However, the procedure relies on CSI. In [18], the authors analyze the performance of a RIS-assisted RA using successive interference cancellation (SIC) for uncoordinated transmission attempts from two transmitters demonstrating that the RIS can help achieve better performance. Nevertheless, the work also lacks the systematical aspects behind a protocol. To address these problems, in [19], we have proposed the initial version of a grant-free RA protocol for multiple uncoordinated UEs considering the scenario in Fig. 1. In there we have shown substantial gains in integrating the RIS into the RA protocol design, but we have omitted several engineering details of the protocol, important for the overall system design. In this work, we extend our protocol presented in [19] by making the following contributions:

- We propose a *channel oracle* enabled by the RIS, which allows each UE to predict the conditions of the channel in the access slots when it wants to attempt to access the network based on a comparatively short training phase. The procedure exploits the RIS's capability of manipulating the environment to bring some coordination to the UEs, enabling them to opportunistically decide when to transmit. The channel oracle works in two steps: a) a training step, and b) an inference step.
- We then propose a grant-free RA protocol with channel oracle, which is comprised of three phases: i) a downlink (DL) training phase, which implements the training step of the channel oracle, ii) an uplink (UL) access phase, which uses the inference step of the channel oracle to come up with access policies that dictate how the UEs chose how to access, and iii) a DL acknowledgment (ACK) phase, which comprehends the feedback channel between the AP and successfully detected UEs.

- We carefully design each of the phases to account for the presence of the RIS and exploit its capabilities of environment control. The key design objectives are to enable a short DL training phases and a longer UL access phases, while getting a satisfactory RIS-assisted ACK method. These characteristics reduce the training overhead and improve the system throughput.

Our grant-free RA protocol aims to efficiently integrate RIS with the ultimate goal of maximizing throughput, which is intrinsically behind the design of each of the phases. We numerically show that our grant-free RA protocol increases the expected end-to-end throughput of the network by approximately 40% when compared to the regular repetition slotted ALOHA (RRS-ALOHA).

The remainder of the paper is organized as follows. In Section II, we introduce our system model based on the setup in Fig. 1. In addition to that, we present the channel model used, the channel oracle principle, and the CC characteristics. Section III gives an overall overview of the proposed RA protocol by defining each one of its phases. The detailed design of each phases can be found in Sections IV-VI. We numerically evaluate our protocol in Section VII, whereas Section VIII draws ours main conclusion.

Notation. The set of positive integers, positive real, real, and complex numbers are denoted by \mathbb{Z}_+ , \mathbb{R}_+ , \mathbb{R} , and \mathbb{C} , respectively. Integer sets are denoted by calligraphic letters $\mathcal{A} = \{0, 1, \dots, A - 1\}$ with cardinality $|\mathcal{A}| = A$. The circularly-symmetric complex Gaussian distribution is $\mathcal{N}_{\mathbb{C}}(\mu, \sigma^2)$ with mean μ and variance σ^2 . Lower and upper case boldface letters denote column vectors \mathbf{x} and matrices \mathbf{A} , respectively. The identity matrix of size N is \mathbf{I}_N and $\mathbf{0}$ is a vector of zeros. Euclidean norm of \mathbf{x} is $\|\mathbf{x}\|_2$. Superscript $(\cdot)^*$ denotes complex conjugate. The $\arg \max(\cdot)$ function returns the index of the maximum element of a vector, while $\text{med}\{\cdot\}$ and $\max\{\cdot\}$ denote the median and the maximum operator over a set, respectively.

II. SYSTEM MODEL

We consider the grant-free RA problem where K single-antenna UEs attempt to deliver payload data to a single-antenna AP at a given RA frame. We let \mathcal{K} denote the set of contending UEs in a frame and assume that the number of contending UEs $|\mathcal{K}| = K$ is distributed according to a Poisson distribution with parameter κ being the *channel load* [20], that is, $K \sim \text{Pois}(\kappa)$. Moreover, we assume that the data packets, sent by the UEs in a grant-free manner, contain at least the UE's identifier, payload data, and cyclic redundancy check (CRC) bits to handle decoding errors. The system operates in a time-division duplex (TDD) mode with DL and UL

directions. The wireless signal has carrier frequency f_c and corresponding wavelength λ with wavenumber $\omega = \frac{2\pi}{\lambda}$.

Fig. 1 depicts the geometry of the considered system setup, where the AP and UEs are points located solely in the x - y -plane. The UEs are uniformly distributed within the indicated area with their LoS paths towards the AP obstructed. Thus, an RIS is strategically positioned to assist the communication between the AP and UEs, where the center of the RIS is assumed to be the origin of our coordinate system. We denote as $\theta_a \in [0, \pi/2]$ the angle between the line normal to the origin and the AP and as $\theta_k \in [0, \pi/2]$ the equivalent angle with respect to the k -th UE. The corresponding distances are denoted as $d_a \in [d_{\min}, d_{\max}]$ and $d_k \in [d_{\min}, d_{\max}]$, where d_{\min}, d_{\max} denote the minimum and maximum distances.

The RIS is formed by $M_x \in \mathbb{Z}_+$ and $M_z \in \mathbb{Z}_+$ wavelength-scale elements disposed as a planar array over the x - and z -dimensions, totaling $M = M_x M_z$ elements. Let \mathcal{M}_x and \mathcal{M}_z be the index sets of the RIS elements over the x - and z -axis, respectively, with $|\mathcal{M}_x| = M_x$ and $|\mathcal{M}_z| = M_z$. Each element has an area of $d_x d_z$ with $d_x, d_z \in \mathbb{R}_+$ and $d_x, d_z \leq \lambda$, which is realized as a metalized layer on a grounded substrate. The dimensions of the RIS are then $D_x = M_x d_x$ and $D_z = M_z d_z$. Moreover, we assume that each RIS element works in an idealistic passive way by inducing a stable phase shift on the incident wave without affecting its amplitude. We let the phase shift impressed by the (m, m') -th element be denoted as $\phi_{m,m'} \in [0, 2\pi]$, $\forall m \in \mathcal{M}_x, \forall m' \in \mathcal{M}_z$.

A. Channel Model

When an incident wave reaches the RIS, it is reflected according to the phase shifts imprinted by the RIS' elements at a given time. We will analyze the electromagnetic signals related to this reflection considering the far-field regime, which assures the plane-wave propagation in the AP-RIS and RIS-UEs paths; this translates to the condition of $d_{\min} = \frac{2}{\lambda} \max(D_x^2, D_z^2)$ [21]. Without loss of generality, we also assume a transverse electromagnetic mode propagation [21], where the electromagnetic waves propagate within the plane perpendicular to the z -axis. As a consequence, the elements with the same index over the z -dimension impress the same phase shift. Hence, for notation convenience, the dependency with the z -dimension can be dropped as $\phi_{m,m'} = \phi_{m,m''} = \phi_m, \forall m' = m'', m', m'' \in \mathcal{M}_z$. We can now provide a channel model for the equivalent channel linking the AP to a UE considering the reflection made by the RIS. For convenience, we denote the phase shifts impressed by the elements during the DL as $\phi^{\text{DL}} \in$

$[0, 2\pi]^{M_x}$ and during the UL as $\phi^{\text{UL}} \in [0, 2\pi]^{M_x}$. By assuming LoS paths linking the AP, a , to the RIS, and the RIS to a UE k , the DL channel response $\zeta_k^{\text{DL}}(\phi^{\text{DL}}) \in \mathbb{C}$ is:

$$\zeta_k^{\text{DL}}(\phi^{\text{DL}}) = \sqrt{\beta_k^{\text{DL}}} e^{j\omega\psi_k} \mathbf{A}_k(\phi^{\text{DL}}), \quad (1)$$

where (ϕ^{DL}) denotes the dependency on the phase shifts; the DL pathloss $\beta_k^{\text{DL}} \in \mathbb{R}_+$ is

$$\beta_k^{\text{DL}} = \frac{G_a G_k}{(4\pi)^2} \left(\frac{d_x d_z}{d_a d_k} \right)^2 \cos^2 \theta_a \quad (2)$$

with G_a and G_k being the antenna gain of the AP and of the UE, respectively. The propagation phase shift $\psi_k \in [0, 2\pi]$ is given by

$$\psi_k = - \left(d_a + d_k - (\sin \theta_a - \sin \theta_k) \frac{M_x + 1}{2} d_x \right). \quad (3)$$

The array factor arising from the discretization of the RIS into a finite number of elements is:

$$\mathbf{A}_k(\phi^{\text{DL}}) = M_z \sum_{m \in \mathcal{M}_x} e^{j(\omega d_x (m+1) (\sin \theta_k - \sin \theta_a) + \phi_m^{\text{DL}})}, \quad (4)$$

where $\phi_m^{\text{DL}} \in [0, 2\pi]$ is the m -th element of ϕ^{DL} . So, the UL channel response $\zeta_k^{\text{UL}}(\phi^{\text{UL}}) \in \mathbb{C}$ is

$$\zeta_k^{\text{UL}}(\phi^{\text{UL}}) = \sqrt{\beta_k^{\text{UL}}} e^{-j\omega\psi_k} \mathbf{A}_k(\phi^{\text{UL}}), \quad (5)$$

where the UL pathloss $\beta_k^{\text{UL}} \in \mathbb{R}_+$ is

$$\beta_k^{\text{UL}} = \frac{G_a G_k}{(4\pi)^2} \left(\frac{d_x d_z}{d_a d_k} \right)^2 \cos^2 \theta_k. \quad (6)$$

The interested reader can check more details about the derivation of the above model in [19]. It is worth pointing out that the antenna array model adopted here can be extended to include the near-field of the RIS through recently proposed plane wave expansion methods [3].

B. Phase-Shift Configurations

In general, we refer to a vector of phase shifts $\phi \in [0, 2\pi]^{M_x}$ as a *phase-shift configuration*, or *configuration* for short. Each configuration can be related to the angle of the resulting reflected wave obtained when the elements simultaneously imprint their phase shifts accordingly. Specifically, if the desired reflecting angle is $\theta_r \in [0, \pi/2]$, we then say that θ_r is realizable by a given configuration ϕ . Moreover, we consider that the RIS is only able to perform a finite

number of reflections since it has a corresponding finite set of predefined configurations.¹ Let $N \in \mathbb{Z}_+$ denote such a finite number and \mathcal{N} its index set. Denote as $\Phi = \{\phi[n]\}_{n \in \mathcal{N}}$ the finite set of configurations or *configuration codebook* and as $\Theta = \{\theta_r[n]\}_{n \in \mathcal{N}}$ the corresponding set of reflecting angles, where we used $[n]$ to index the elements of the sets Φ and Θ based on classical signal processing literature [22] as a notation convenience. Thus, the RIS reflecting capability can mathematically be defined as the bijection function

$$h : \Phi \mapsto \Theta. \quad (7)$$

We now provide the design of the mapping h to get a desired θ_r from ϕ . This process is divided into analyzing the DL and UL transmission directions independently since the direction of the incoming wave towards the RIS changes accordingly. As a consequence, we introduce the notation θ_r^{DL} and θ_r^{UL} to denote the reflecting angles during each direction. In the DL, the AP sends a signal towards the RIS, whose incoming direction is θ_a ; then, the AP controls the RIS to reflect the incoming signal towards a desired reflecting direction θ_r^{DL} based on a configuration ϕ^{DL} . Observe that the reflecting angle θ_r^{DL} represents a possible direction in which a UE can be located since the AP does not know the UEs's angular positions θ_k . In the UL, the incoming signals come from random directions θ_k . Due to the lack of angular position information, the best the AP can guess is that the incoming waves are coming from the reflecting directions θ_r^{DL} 's used during the DL. Then, the AP controls the RIS to reflect the guessed incoming waves towards its direction, that is, $\theta_r^{\text{UL}} = \theta_a$. Therefore, the configuration design can be written as [23]:

$$\phi_m^{\text{DL}} = \omega d_x (m+1)(\sin \theta_a - \sin \theta_r^{\text{DL}}) \quad \text{and} \quad \phi_m^{\text{UL}} = \omega d_x (m+1)(\sin \theta_r^{\text{DL}} - \sin \theta_a), \quad \forall m \in \mathcal{M}_x. \quad (8)$$

Hence, one can note that $\phi_m^{\text{DL}} = -\phi_m^{\text{UL}}$ since $\theta_r^{\text{UL}} = \theta_a$. This design can also be obtained based on the Generalized Snell's Law [24]. By substituting (8) into (4), the array factor becomes:

$$\mathbf{A}_k(\phi^{\text{DL}}) \equiv \mathbf{A}_k(\theta_r^{\text{DL}}) = M_z \sum_{m \in \mathcal{M}_x} e^{j\omega d_x (m+1)(\sin \theta_k - \sin \theta_r^{\text{DL}})}. \quad (9)$$

Observe that $\mathbf{A}_k(\phi^{\text{UL}}) = \mathbf{A}_k^*(\phi^{\text{DL}})$. As a result, the channel responses are also a function of the reflecting angle θ_r^{DL} used during the DL, that is, it is equivalent to say that $\zeta_k^{\text{DL}}(\phi^{\text{DL}}) \equiv \zeta_k^{\text{DL}}(\theta_r^{\text{DL}})$.

¹For convenience, we have assumed that the phase shifts can take any value in the continuous interval, *i.e.*, $\phi_m \in [0, 2\pi]$. Due to hardware constraints, each element can only induce a phase shift whose value comes from a finite set [6]. The results provided here can be seen as an upper bound in terms of performance since finite precision would result in unavoidable quantization error.

C. AP-RIS Control Channel

We consider that the AP controls the operation of the RIS through a dedicated out-of-band CC, *i.e.*, the RIS control does not interfere with the wireless signals exchanged between the AP and UEs [5]. For convenience, we also assume that the CC is error-free. Thus, the AP sends command messages to the RIS consisting of the desired configuration to be loaded by the RIS at a given time slot. The command messages are interpreted by the RIS controller (RIS-C) which is equipped with a look-up table containing the configuration indexes in \mathcal{N} ; it is assumed that the equivalent mapping $h' : \mathcal{N} \mapsto \Theta$ is previously exchanged and known at both ends. After the RIS receives a configuration change command, it needs a physical switching time of T_{sw} seconds to load the new configuration. The AP remains silent during this time in the DL, while it ignores any signal received during the switching time in the UL.

D. Channel Oracle

In this part, we introduce the *channel oracle* enabled by the RIS and used as a basis for our proposed protocol. It is named in this way because the RIS enables the UEs to opportunistically predict when they should attempt to access the AP assuming channel reciprocity. Conceptually, the channel oracle is comprised of two steps: i) a DL training step and ii) a UL inference step, as illustrated in Fig. 2. During the first step, the AP sends reference signals towards the UEs, while it controls the RIS to sweep over a meticulously designed set of DL reflecting angles, namely, the training codebook, denoted as $\Phi_{\text{tr}} \equiv \Theta_{\text{tr}}$ and enumerated by \mathcal{N}_{tr} , $|\mathcal{N}_{\text{tr}}| = N_{\text{tr}}$. After this operation, the UEs are able to sample, estimate, and then reconstruct their own model for the DL channel response function $\hat{f}_k : \theta_r^{\text{DL}} \mapsto \hat{\zeta}_k^{\text{DL}}$ as defined in (1) and (8) by using reconstruction methods based on classical signal processing techniques [22]. During the UL inference step, the AP designs a new set of UL reflecting angles, namely, the access codebook, denoted as $\Phi_{\text{ac}} \equiv \Theta_{\text{ac}}$ and enumerated by \mathcal{N}_{ac} , $|\mathcal{N}_{\text{ac}}| = N_{\text{ac}}$. The AP sweeps over the access codebook, delimiting access slots in which the UEs can attempt to send their messages. Considering that the information about the RA frame is broadcasted beforehand by the AP, the UEs can predict what the UL channel responses will be when they want to access the network, knowing the defined access codebook and assuming channel reciprocity [23]. From an engineering point of view, we want N_{tr} to be as small as possible while the reconstruction \hat{f} meets a given error tolerance and helps the UEs to achieve a specified access performance for a given size of the access block, N_{ac} . Moreover, it is desired to have $N_{\text{ac}} \gg N_{\text{tr}}$ so as to reduce the training overhead.

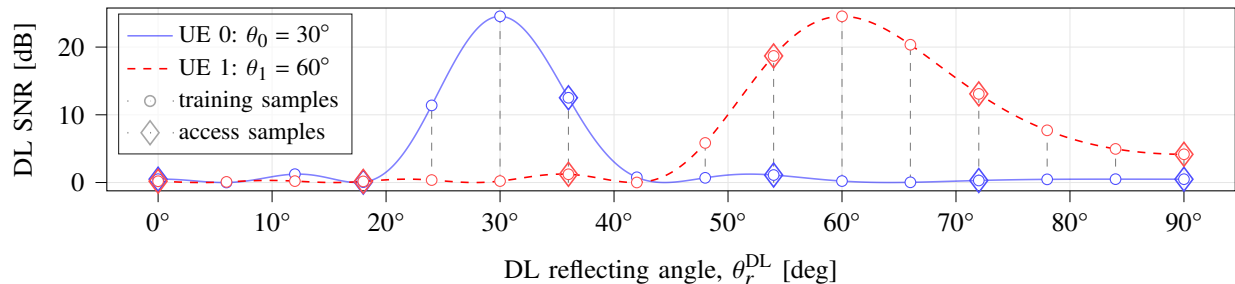


Fig. 2. Illustration on how the channel oracle samples the channel in each step when considering two UEs with $N_{\text{tr}} = 16$ number of training configurations and $N_{\text{ac}} = 6$ number of access configurations.

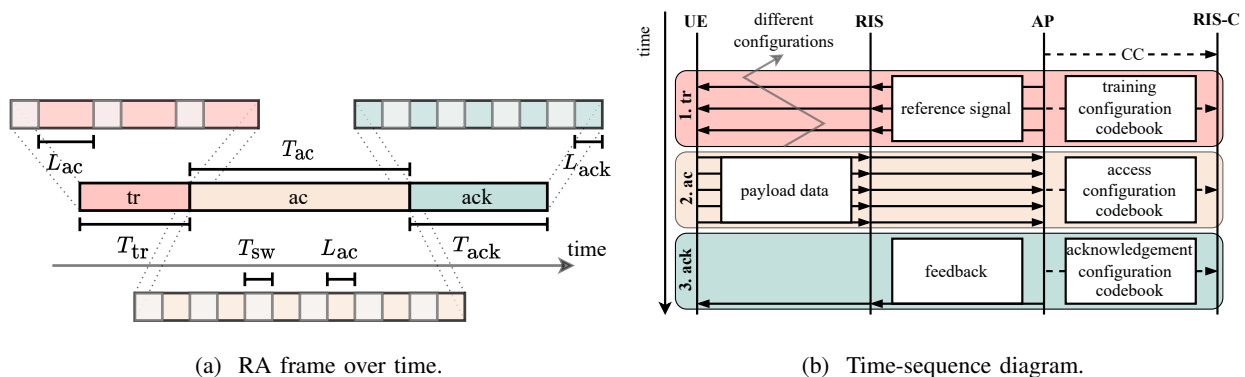


Fig. 3. Proposed grant-free RA protocol for RIS-aided systems. Training, access, and acknowledgment are abbreviated as tr, ac, and ack for indexing, respectively. For $i \in \{\text{'tr'}, \text{'ac'}, \text{'ack'}\}$, T_i represents the duration of each phase, while L_i represents the duration of the respective time slots in terms of channel uses. The switching time of the RIS is T_{sw} . In the time-sequence diagram, the dashed arrow denotes communication occurring over the CC, while the solid arrows denote the sweeping process.

III. THE DESIGN OF THE RANDOM ACCESS PROTOCOL

The key contribution of this paper is the design of a RA protocol suited for scenarios where an RIS extends the coverage of an AP, as illustrated in Fig. 1. In this section, we provide an overview of the protocol by firstly defining its corresponding RA frame and, then, describing how it defines the exchange of messages, actions, and decisions taken by the communication entities over time.

We consider the frame structure shown in Fig. 3a based on time-division multiple access (TDMA). The frame is comprised of a DL training (tr) phase of duration T_{tr} , a UL access (ac) phase of duration T_{ac} , and a DL acknowledgment (ack) phase of duration T_{ack} . Hence, the total duration of the frame is $T = T_{\text{tr}} + T_{\text{ac}} + T_{\text{ack}}$. We assume that the coherence time of the channel is larger than the frame duration T , following the phase-fading model [25]. Moreover, each phase

is further divided into time slots, where the number of time slots is respectively denoted as C_{tr} , C_{ac} , and C_{ack} . The length of a time slot is measured in terms of channel uses, which corresponds to the number of samples in which a signal is observed within a time slot. Thus, we have the following relationship:

$$T_i = C_i L_i + \xi_i C_i T_{\text{sw}}, \quad (10)$$

where $i \in \{\text{'tr'}, \text{'ac'}, \text{'ack'}\}$, L_i denotes the corresponding number of channel uses, and $\xi_i C_i T_{\text{sw}}$ takes into account the switching time coming from the controlling process of changing the RIS' configurations. We denote as $\xi_i \in [0, 1]$ the ratio of the number of configuration changes that occur within a phase to the number of time slots that form that phase. We now give a general overview of the operation of the proposed protocol over time, as illustrated in Fig. 3b.

A. Downlink Training Phase

The DL training phase implement the training step of the channel oracle and is comprised of a single element as follows:

- 1) *Training codebook*: AP designs a first configuration codebook $\Phi_{\text{tr}} \equiv \Theta_{\text{tr}}$ as per (7) enumerated by \mathcal{N}_{tr} . In particular, we assume that the number of training slots is equal to the number of training configurations, *i.e.*, $C_{\text{tr}} = N_{\text{tr}}$ with $N_{\text{tr}} = |\mathcal{N}_{\text{tr}}|$. The AP broadcasts training signals over the entire duration of the training phase, while it controls the RIS to change its configuration at each slot by sequentially going through the configurations enumerated by \mathcal{N}_{tr} . The UEs are then able to obtain a model $\hat{f}_k : \theta_r^{\text{DL}} \mapsto \hat{\zeta}_k^{\text{DL}}$ to predict their UL channel.

B. Uplink Access Phase

The UL access phase performs the inference step of the channel oracle and is comprised of mainly three elements as follows:

- 1) *Access codebook*: AP designs a second configuration codebook $\Phi_{\text{ac}} \equiv \Theta_{\text{ac}}$ enumerated by \mathcal{N}_{ac} . As before, we assume that the number of access slots is equal to the number of access configurations, *i.e.*, $C_{\text{ac}} = N_{\text{ac}}$ with $N_{\text{ac}} = |\mathcal{N}_{\text{ac}}|$. This access codebook is shared to the UEs. Each UE is then able to evaluate the access slots using its model \hat{f}_k obtained during the training phase.
- 2) *Access policy*: Based on the predicted channel responses, each UE chooses the access slots to transmit according to access policies. In principle, an access policy wants to select the

access slots that are most likely to ensure successful transmission of a UE. In general, we consider that an access policy can select more than one access slot to achieve its objective.

- 3) *AP Decoder*: AP collects all the packets sent by the UEs according to an access policy and starts the decoding process. We consider that the AP employs a decoder that makes use of a collision resolution strategy as follows. First, the AP decodes the singleton access slots, *i.e.*, access slots in which only a single UE has sent a packet. Secondly, the AP repeatedly uses SIC to attempt to recover other non-singleton packets (see further details in [19, Algo. 1]). The decoding process is repeated until there are no more slots or the AP is not able to resolve collisions. Moreover, a packet is only considered successfully decoded by the AP if the UL received signal-to-noise ratio (SNR) of a given UE is above a certain minimum threshold, $\gamma_{ac} \in \mathbb{R}_+$. Consequently, only the subset of UEs $\mathcal{K}_{ac} \subseteq \mathcal{K}$ has its signal successfully decoded by the AP with $|\mathcal{K}_{ac}| = K_{ac}$.

C. Downlink Acknowledgment Phase

The DL ACK phase informs UEs in \mathcal{K}_{ac} that their packet have been successfully decoded. However, different from traditional ACK, the ACK procedure now needs to be aware and take advantage of the RIS. The DL ACK phase is comprised of two elements as follows:

- 1) *ACK codebook*: AP designs a third configuration codebook $\Phi_{ack} \equiv \Theta_{ack}$ enumerated by N_{ack} with $N_{ack} = |\mathcal{N}_{ack}|$. Herein, the goal is to ensure that the K_{ac} successfully decoded UEs get their ACKs with a high probability of decoding it successfully. Thus, we consider a simple ACK strategy in which the number of ACK slots is equal to the number of UEs successfully decoded by the AP, *i.e.*, $C_{ack} = K_{ac}$. In particular, we will propose two heuristic approaches to design the ACK configuration codebook: i) precoding-based and ii) TDMA-based. According to those, the AP sends the ACKs to the UEs while controlling the RIS configurations. Each ACK message contains at least the identity of its corresponding UE.
- 2) *ACK check*: We consider that an ACK is only successful if and only if the DL received SNR is above a certain threshold, $\gamma_{ack} \in \mathbb{R}_+$. Thus, only the subset of UEs, $\mathcal{K}_{ack} \subseteq \mathcal{K}_{ac}$ that successfully received the ACKs will be satisfied and will end the access attempts. The subset of unsuccessful UEs, $\mathcal{K}_{un} = \mathcal{K} \setminus \mathcal{K}_{ack}$ may retry access in future RA frames.

D. Practical Control Considerations

In a practical system, the RA frame would be repeated with a certain frequency configured by the network, which can be dependent on an estimate of the channel load κ . We note the AP just needs to determine and calculate the training and access codebooks for a long time horizon; for example, until the channel load κ changes. For that reason, the AP can broadcast the RA frame information less often. Throughout this information, the UEs have access to the corresponding training and access mappings $h'_{\text{tr}} : \mathcal{N}_{\text{tr}} \mapsto \theta_{\text{tr}}$ and $h'_{\text{ac}} : \mathcal{N}_{\text{ac}} \mapsto \theta_{\text{ac}}$ at their side. On the other hand, one should observe that the equivalent ACK mapping does not need to be known by the UEs in advance. Given the protocol description, the ratio ξ_i in (10) evaluates to: $\xi_{\text{tr}} = \xi_{\text{ac}} = 1$, $\xi_{\text{ack}}^{\text{prec}} = 1/C_{\text{ack}}$ for the precoding-based ACK, and $\xi_{\text{ack}}^{\text{prec}} = 1$ for the TDMA-based ACK. In the following sections, we further detail the design of each one of the phases.

IV. DOWNLINK TRAINING PHASE

In this section, we detail the design of the DL training phase. First, we propose a way to devise the training configuration codebook based on a signal processing interpretation of the DL channel response defined in (1). The design the codebook is based on the Nyquist-Shannon theorem [22], enabling the UEs to collect the minimum number of spatial samples required to locally reconstruct the DL channel response function perfectly under noiseless conditions. Then, we characterize the DL training signals received by the UEs and discuss a way to determine the number of channel uses L_{tr} so as to combat the noise effect. Finally, we show how each UE gets a model $\hat{f}_k : \theta_r^{\text{DL}} \mapsto \hat{\zeta}_k^{\text{DL}}$ according to the channel oracle.

A. Training Configuration Codebook

We start by interpreting the DL channel response in (1) as a signal that continuously varies over time, t , due to wireless transmission, and over the reflected-angular space, θ_r^{DL} , or simply space. Accordingly, we rewrite (1) as:

$$\zeta_k^{\text{DL}}(t, \theta_r^{\text{DL}}) = \sqrt{\beta_k^{\text{DL}}(t)} e^{j\omega\psi_k(t)} \mathbf{A}_k(t, \theta_r^{\text{DL}}(t)), \quad (11)$$

which is a complex-valued, multidimensional signal continuous over time $t \in (-\infty, +\infty)$ and space $\theta_r^{\text{DL}}(t) \in [0, \pi/2]$. For convenience, we remove the time domain by making the following argument. Because of TDMA, let us assume that the time domain can be discretized over infinitely many time slots. Consider that θ_r^{DL} can only change once in each time slot, that is, we

can only switch a single configuration per slot. Therefore, for the sake of the analysis, the time domain can be folded onto the space domain, while ensuring continuity of the latter. Thus, the signal can be expressed as:

$$\zeta_k^{\text{DL}}(\theta_r^{\text{DL}}) = \sqrt{\beta_k^{\text{DL}}} e^{j\omega\psi_k} M_z \sum_{m \in \mathcal{M}_x} e^{j\omega d_x(m+1)(\sin\theta_k - \sin\theta_r^{\text{DL}})}. \quad (12)$$

By substituting β_k^{DL} in (2), ψ_k in (3), and $\omega = \frac{2\pi}{\lambda}$, we get

$$\zeta_k^{\text{DL}}(\theta_r^{\text{DL}}) = \underbrace{\left(\sqrt{\beta_k^{\text{DL}}} M_z\right)}_{\text{Term 1}} \underbrace{e^{j2\pi F_0 \left(\frac{da+dk}{d_x} - \frac{M_x+1}{2}(\sin\theta_a - \sin\theta_k)\right)}}_{\text{Term 2}} \underbrace{\sum_{m \in \mathcal{M}_x} e^{j2\pi F_0(m+1)(\sin\theta_k - \sin\theta_r^{\text{DL}})}}_{\text{Term 3, } a_k(\theta_r^{\text{DL}})}, \quad \theta_r^{\text{DL}} \in \left[0, \frac{\pi}{2}\right].$$

Clearly, the signal above is periodic over space with fundamental spatial frequency and fundamental spatial period respectively given by:

$$F_0 = \frac{d_x}{\lambda}, \quad \text{and} \quad T_p = \frac{\lambda}{d_x}. \quad (13)$$

Note that typically $d_x = o(\lambda)$, consequently $F_0 \leq 1$ Hz; meaning that we are dealing with a very slowly varying spatial signal. One should keep in mind that the above signal is also random, due to the unknown position of the UE described by the random variables d_k and θ_k .

We now study the analog signal $\zeta_k^{\text{DL}}(\theta_r^{\text{DL}})$ in (12) by performing a spatial frequency analysis. The key idea is that the AP can design the set of configurations Φ_{tr} by discretizing $\zeta_k^{\text{DL}}(\theta_r^{\text{DL}})$ over the spatial domain according to the corresponding reflection angles in Θ_{tr} such that each UE can locally reconstruct its analog signal $\zeta_k^{\text{DL}}(\theta_r^{\text{DL}})$ based on sampling theory [22], [26]. For this purpose, we analyze the spatial frequency of Term 3, namely $a_k(\theta_r^{\text{DL}})$, since the other two are independent of θ_r^{DL} . Let F_{max} denote the maximum spatial frequency of $a_k(\theta_r^{\text{DL}})$, or, equivalently, of $\zeta_k^{\text{DL}}(\theta_r^{\text{DL}})$. Our goal is to characterize this frequency so that we can apply the Nyquist-Shannon theorem [22]. However, the form of $a_k(\theta_r^{\text{DL}})$ does not allow for an analytical treatment and, hence, we resorted to two approximated methods, which are given below.

1) *Finding the maximum frequency using Taylor series:* By using the first term of the Taylor series expansion $\sin x = x + \mathcal{O}(x^3)$, we approximate $a_k(\theta_r^{\text{DL}})$ as:

$$\tilde{a}_k(\theta_r^{\text{DL}}) \approx \sum_{m \in \mathcal{M}_x} e^{j2\pi F_0(m+1)(\sin\theta_k - \theta_r^{\text{DL}})}. \quad (14)$$

The above signal can be seen as a set of harmonically related complex exponentials [22], whose component with the highest spatial frequency is related to the M_x -th complex exponential with

$$\tilde{F}_{\text{max}} = M_x F_0 = M_x \frac{d_x}{\lambda} = \frac{D_x}{\lambda}, \quad (15)$$

where recall that D_x is the horizontal dimension of the RIS.

2) *Finding the maximum frequency using power conservation efficiency:* One can note that the approximation above is only good for very small values of θ_r^{DL} . So, we need to look for a better way of approximating F_{\max} . Since the signal is periodic, another form to represent it would be to obtain its Fourier series. To do so, we first rewrite $a_k(\theta_r^{\text{DL}})$ in (12) as

$$a_k(\theta_r^{\text{DL}}) = \left(\sum_{m \in \mathcal{M}_x} e^{j2\pi F_0(m+1)(\sin \theta_k - \sin \theta_r^{\text{DL}})} \right) u(\theta_r^{\text{DL}}), \quad (16)$$

where $u(\theta_r^{\text{DL}})$ is the rectangular function with $u(\theta_r^{\text{DL}}) = 1$ if $\theta_r^{\text{DL}} \in [0, \pi/2]$ and 0 otherwise. We then remark that the Fourier series of the signal exists because it satisfies the weak Dirichlet conditions [22], having finite energy in one period. Thus, the Fourier series of $a_k(\theta_r^{\text{DL}})$ can be written as [22]:

$$a_k(\theta_r^{\text{DL}}) = \sum_{i=-\infty}^{\infty} c_k(i) e^{j2\pi i F_0 \theta_r^{\text{DL}}}, \quad (17)$$

whose coefficient $c_k(i) \in \mathbb{C}$ is calculated as

$$c_k(i) = \frac{1}{T_p} \int_0^{T_p} a_k(\theta_r^{\text{DL}}) e^{-j2\pi i F_0 \theta_r^{\text{DL}}} d\theta_r^{\text{DL}} = \frac{1}{T_p} \sum_{m \in \mathcal{M}_x} e^{j2\pi F_0(m+1) \sin \theta_k} \int_0^{\frac{\pi}{2}} e^{-j2\pi F_0((m+1) \sin \theta_r^{\text{DL}} + i \theta_r^{\text{DL}})} d\theta_r^{\text{DL}}. \quad (18)$$

Unfortunately, the integral above does not admit a closed-form solution and we had to resort to numerical solutions. With the Fourier series of the signal of interest in hand, we now evaluate its finite average power as follows [22]

$$P_{a_k} = \frac{1}{T_p} \int_0^{T_p} |a_k(\theta_r^{\text{DL}})|^2 d\theta_r^{\text{DL}} \stackrel{(a)}{\leq} \frac{1}{T_p} \int_0^{\frac{\pi}{2}} \left(\sum_{m \in \mathcal{M}_x} \left| e^{j2\pi F_0(m+1)(\sin \theta_k - \sin \theta_r^{\text{DL}})} \right| \right)^2 d\theta_r^{\text{DL}} = M_x^2, \quad (19)$$

where in (a) we used the subadditivity property of the absolute value. As expected, this result gives us an upper bound for the value of Term 3 in Eq. (12), which meets the expected array gain of M_x coming from the RIS elements along the x -dimension. Based on average power conservation, we propose a heuristic approach to approximate the maximum spatial frequency of the signal. First, by the Parseval's relation [22] and the above result, we have that

$$P_{a_k} = \sum_{i=-\infty}^{\infty} |c_k(i)|^2 \leq M_x^2. \quad (20)$$

Let $0 \leq \epsilon \leq 1$ parameterize the notion of conservation efficiency of the average power, *i.e.*, the percentage of the error we commit due to the approximation. The smallest symmetric interval of the coefficients of the series that ensure the desired power efficiency is

$$\text{find } I_k^\epsilon \in \mathbb{Z}_+ \text{ s.t. } \sum_{i=-I_k^\epsilon}^{I_k^\epsilon} |c_k(i)|^2 \geq (1 - \epsilon) P_{a_k}, \quad (21)$$

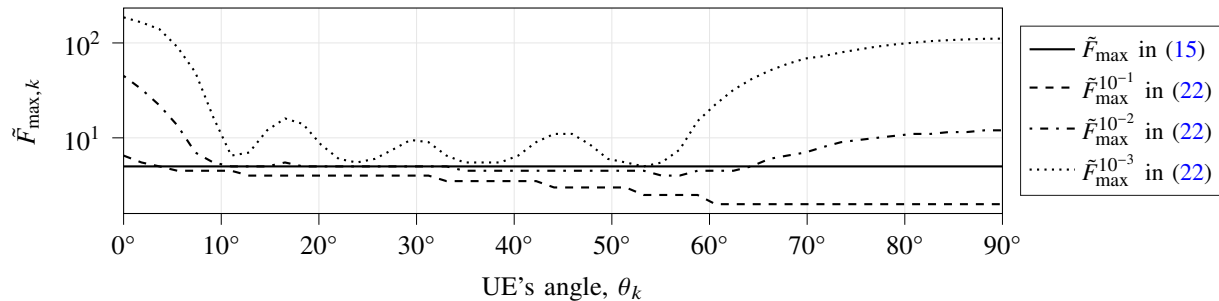


Fig. 4. Evaluation of the two approximations of the maximum frequency of $a_k(\theta_r^{\text{DL}})$ as a function of the UE's angle θ_k and for different values of ϵ with $F_0 = 0.5$ Hz.

where the existence of a solution is ensured by the fact that the infinite sum of coefficients is bounded in (20), $\exists I_k^\epsilon \in \mathbb{Z}_+$, $\forall k$. Thus, the maximum spatial frequency can be approximated as:

$$\tilde{F}_{\max,k}^\epsilon = I_k^\epsilon \cdot F_0, \quad (22)$$

where $F_{\max} \geq \tilde{F}_{\max,k}^\epsilon$ with equality when $\epsilon \rightarrow 0$. In practice, F_0 is fixed, while I_k^ϵ depends on the UE's position through θ_k .

3) *Evaluating the maximum spatial frequency:* The two approximated methods proposed are evaluated in Fig. 4 as a function of the UE's angles, with ϵ having values 10^{-1} , 10^{-2} , and 10^{-3} , and with a fundamental frequency of $F_0 = 0.5$ Hz. In addition, the approximation obtained via Taylor series in (15) evaluates as $\tilde{F}_{\max} = M_x F_0 = 50$ Hz, $\forall k$. The figure shows that the maximum frequency is highly dependent on the position of the UEs, which is undesired from the standpoint of the AP since it is unaware of the UEs positions in advance. For this reason, we evaluate statistics of $\tilde{F}_{\max,k}$ over θ_k that are going to be relevant in the sequel. The median with respect to θ_k yields in: $\check{F}_{\max}^{10^{-1}} = 3.0$ Hz, $\check{F}_{\max}^{10^{-2}} = 5.0$ Hz, and $\check{F}_{\max}^{10^{-3}} = 14.5$ Hz. On the other hand, the maximum with respect to the angle θ_k yields in: $\check{F}_{\max}^{\check{10^{-1}}} = 6.5$ Hz, $\check{F}_{\max}^{\check{10^{-2}}} = 45.0$ Hz, and $\check{F}_{\max}^{\check{10^{-3}}} = 186.0$ Hz. One can also note that the Taylor-based method in (15) actually yields an approximation of F_{\max} similar to $\check{F}_{\max}^{10^{-2}}$ when $\epsilon = 10^{-2}$, showing consistency despite the rough approximation. In summary, we conclude that characterizing the maximum spatial frequency F_{\max} of the signal $a(\theta_r^{\text{DL}})$ highly depends on the UE's position and the amount of signal power that one wants to conserve, which is controlled by the selection of ϵ . The smaller the ϵ , the better the characterization of the maximum spatial frequency, and thus the signal will be better discretized according to the Nyquist-Shannon theorem [22], allowing a better reconstruction of the signal of interest at the UE's side.

4) *Nyquist-Shannon Theorem*: We now define the training configuration codebook Φ_{tr} based on the Nyquist-Shannon theorem². Let the uniform sampling over space be denoted as [22], [26]

$$\zeta_k^{\text{DL}}[n] = \zeta_k^{\text{DL}}(nT_{\text{samp}}), \quad (23)$$

where $\zeta_k^{\text{DL}}[n]$ is the discrete-time signal obtained by sampling the analog signal $\zeta_k^{\text{DL}}(\theta_r^{\text{DL}})$ with spatial sampling period $T_{\text{samp}} \in \mathbb{R}_+$ and $n \in \mathcal{N}_{\text{tr}}$. Let $F_{\text{samp}} = \frac{1}{T_{\text{samp}}}$ be the spatial sampling frequency. Based on the most general method to determine the maximum spatial frequency in (22), the Nyquist rate that allows perfect reconstruction of the signal is [22]:

$$F_{\text{samp}} \geq 2F_{\text{max}} \implies \tilde{F}_{\text{samp},k}^\epsilon \gtrsim 2F_{\text{max}}^\epsilon = 2I_k^\epsilon F_0 = 2I_k^\epsilon \frac{d_x}{\lambda} = 2 \frac{I_k^\epsilon}{\lambda M_x} D_x, \quad (24)$$

where \gtrsim denotes an approximation of the inequality. The above relationship shows that the approximated sampling frequency $\tilde{F}_{\text{samp},k}^\epsilon$ is directly proportional to the size of the RIS D_x , and depends on the conservation efficiency ϵ , and the UE's position θ_k . Moreover, it is important to note that, since ϵ cannot be made infinitely small, we would always perform some undersampling because of $F_{\text{max}} > \tilde{F}_{\text{max},k}^\epsilon$. Similarly, observe that the above expression can also be written with respect to the Taylor-based approximation in (15), which yields similar conclusions.

Based on (24) and $\theta_r^{\text{DL}} \in [0, \pi/2]$, we obtain an approximated lower bound on the number of samples, or configurations, required to perfectly reconstruct the signal at the k -th UE under a noiseless condition as:

$$\tilde{N}_{\text{tr},k}^\epsilon \geq \left\lceil \frac{\pi}{2} \tilde{F}_{\text{samp},k}^\epsilon \right\rceil = \left\lceil \pi \frac{I_k^\epsilon}{\lambda M_x} D_x \right\rceil = \lceil \pi I_k^\epsilon F_0 \rceil \in \mathbb{Z}_+. \quad (25)$$

As observed before, the problem of using the above result to design the training codebook is its dependence on the UEs' positions, which are unknown to the AP. Thus, we consider three different statistical criteria to get feasible lower bounds that are independent of the UEs position and would heuristically and statistically ensure good, but different, reconstruction performances:

- *Median*: choose $\hat{N}_{\text{tr}}^\epsilon = \text{med}_k \{\tilde{N}_{k,\text{tr}}^\epsilon\}$, *i.e.*, statistically, half of the UEs will have their true lower bound in (25) respected.
- *Maximum*: choose $\hat{N}_{\text{tr}}^\epsilon = \max_k \{\tilde{N}_{k,\text{tr}}^\epsilon\}$, *i.e.*, all the UEs will have their true lower bound in (25) respected, but at the price of increased duration of the training phase due to overly oversampling for most of the UEs.

²In RIS literature, it is worth mentioning that Nyquist sampling rate is also used in connection with accurate near field channel modeling [4], [27], which is totally different from the way we have applied.

- *Taylor-approximation*: choose \tilde{N}_{tr} according to (15), whose price is oversampling.

The training configuration codebook design is then:

$$\Theta_{\text{tr}} = \{\theta_r^{\text{DL}}[n] : nT_{\text{samp}}, n \in \mathcal{N}_{\text{tr}}\} \text{ with } \Phi_{\text{tr}} \stackrel{(a)}{=} h^{-1}(\Theta_{\text{tr}}), \quad (26)$$

where $N_{\text{tr}} = |\mathcal{N}_{\text{tr}}|$ can be chosen from the set $\{\tilde{N}_{\text{tr}}^\epsilon, \check{N}_{\text{tr}}^\epsilon, \tilde{N}_{\text{tr}}\}$, with T_{samp} defined accordingly, and, in (a), we used (7). As a numerical example, by assuming $F_0 = 0.5$ Hz, we have: $\tilde{N}_{\text{tr}}^{10^{-2}} = 16$, $\check{N}_{\text{tr}}^{10^{-3}} = 46$, $\tilde{N}_{\text{tr}}^{10^{-2}} = 142$, $\check{N}_{\text{tr}}^{10^{-3}} = 585$, and $\tilde{N}_{\text{tr}} = 150$ configurations.

B. Downlink Received Training Signal

At the beginning of the RA frame, the AP starts transmitting a training signal towards the UEs, while controlling the RIS to sweep through the training codebook designed according to (26). For $n \in \mathcal{N}_{\text{tr}}$, the DL training signal $\mathbf{w}_k[n] \in \mathbb{C}^{L_{\text{tr}}}$ received by the k -th UE is

$$\mathbf{w}_k[n] = \sqrt{\rho_a} \zeta_k^{\text{DL}}[n] \mathbf{v}_{\text{tr}} + \boldsymbol{\eta}_k[n], \quad (27)$$

where ρ_a is the AP transmit power, $\mathbf{v}_{\text{tr}} \in \mathbb{C}^{L_{\text{tr}}}$ represents the training signal with zero mean and $\mathbb{E}\{\|\mathbf{v}_{\text{tr}}\|_2^2\} = L_{\text{tr}}$, and $\boldsymbol{\eta}_k[n] \in \mathbb{C}^{L_{\text{tr}}} \sim \mathcal{N}_{\mathbb{C}}(\mathbf{0}, \sigma^2 \mathbf{I}_{L_{\text{tr}}})$ is the receiver noise with variance σ^2 . We assume that noise is independent and identically distributed (i.i.d.) over n . The final goal of the k -th UE is to reconstruct the analog signal $\zeta_k^{\text{DL}}(\theta_r^{\text{DL}})$ in (12) from the collection of samples $\{\mathbf{w}_k[n]\}_{n \in \mathcal{N}_{\text{tr}}}$. Before doing so, the k -th UE needs to estimate the sampled complex amplitudes $\zeta_k^{\text{DL}}[n]$ from $\mathbf{w}_k[n]$, whose process is summarized in the following corollary.

Corollary 1. *The Cramér-Rao lower bound (CRLB) for the estimation of $\zeta_k^{\text{DL}}[n]$ from $\mathbf{w}_k[n]$ is*

$$\delta_{\text{tol}}^{\text{DL}} \geq \frac{1}{\text{SNR}_a^{\text{DL}} L_{\text{tr}}}, \quad (28)$$

where $\text{SNR}_a^{\text{DL}} = \frac{\rho_a}{\sigma^2}$ is the DL transmit SNR and $\delta_{\text{tol}}^{\text{DL}}$ is a chosen estimation error tolerance. From the CRLB, it is possible to obtain the following minimum variance unbiased estimator:

$$\hat{\zeta}_k^{\text{DL}}[n] = \frac{1}{L_{\text{tr}} \sqrt{\rho_a}} \mathbf{v}_{\text{tr}}^{\text{T}} \mathbf{w}_k[n], \quad (29)$$

which is distributed as $\mathcal{N}_{\mathbb{C}}(\zeta_k^{\text{DL}}[n], \delta_{\text{tol}}^{\text{DL}})$.

Proof. The proof follows the steps in [28, Ch. 13]. □

The number of channel uses L_{tr} can be chose to meet a given estimation performance as:

$$L_{\text{tr}} \geq \left\lceil \frac{1}{\text{SNR}_a^{\text{DL}} \delta_{\text{tol}}^{\text{DL}}} \right\rceil. \quad (30)$$

C. Channel Oracle – Training Step

Now that the UEs got their estimates $\{\hat{\zeta}_k^{\text{DL}}[n]\}_{n \in \mathcal{N}_{\text{tr}}}$, they can reconstruct their analog signals $\zeta_k^{\text{DL}}(\theta_r^{\text{DL}})$ in (12) and obtain their own model $\hat{f}_k : \theta_r^{\text{DL}} \mapsto \hat{\zeta}_k^{\text{DL}}$. Let $\hat{\zeta}_k^{\text{DL}}(\theta_r^{\text{DL}})$ denote the signal resulting from an interpolation process over the collection of estimates $\{\hat{\zeta}_k^{\text{DL}}[n]\}_{n \in \mathcal{N}_{\text{tr}}}$. Let $\Lambda : [0, \pi/2] \mapsto \mathbb{C}$ be an interpolating function. Then, the reconstructed signal can be written as

$$\hat{\zeta}_k^{\text{DL}}(\theta_r^{\text{DL}}) = \sum_{n \in \mathcal{N}_{\text{tr}}} \hat{\zeta}_k^{\text{DL}}[n] \cdot \Lambda(\theta_r^{\text{DL}} - nT_{\text{samp}}), \forall \theta_r^{\text{DL}} \in \Theta_{\text{tr}}. \quad (31)$$

The above reconstruction can give the parameters necessary to define a model $\hat{f}_k : \theta_r^{\text{DL}} \mapsto \hat{\zeta}_k^{\text{DL}}$ that outputs a $\hat{\zeta}_k^{\text{DL}}$ for any $\theta_r^{\text{DL}} \in [0, \pi/2]$ by using interpolation theory [29]. In the following corollary, we characterize the expected squared error (SE) of the reconstruction with respect to the set of estimates $\{\hat{\zeta}_k^{\text{DL}}[n]\}_{n \in \mathcal{N}_{\text{tr}}}$.

Corollary 2. *The interpolation is distributed according to*

$$\hat{\zeta}_k^{\text{DL}}(\theta_r^{\text{DL}}) \sim \mathcal{N}_{\mathbb{C}} \left(\hat{\zeta}_k^{\text{DL}}(\theta_r^{\text{DL}}), \delta_{\text{tol}}^{\text{DL}} \sum_{n \in \mathcal{N}_{\text{tr}}} \Lambda(\theta_r^{\text{DL}} - nT_{\text{samp}}) \right), \quad (32)$$

where $\hat{\zeta}_k^{\text{DL}}(\theta_r^{\text{DL}}) = \sum_{n \in \mathcal{N}_{\text{tr}}} \hat{\zeta}_k^{\text{DL}}[n] \cdot \Lambda(\theta_r^{\text{DL}} - nT_{\text{samp}})$ denotes the interpolation under a noiseless condition. Moreover, the expected SE of the reconstruction $\mathbb{E}\{|\hat{\zeta}_k^{\text{DL}}(\theta_r^{\text{DL}}) - \zeta_k^{\text{DL}}(\theta_r^{\text{DL}})|^2\}$ is

$$\overline{\text{SE}} = \delta_{\text{tol}}^{\text{DL}} \sum_{n \in \mathcal{N}_{\text{tr}}} \Lambda(\theta_r^{\text{DL}} - nT_{\text{samp}}) + \text{TSE}, \quad (33)$$

where the first term on the right-hand side accounts for the noise and estimation effects, while the second term, namely TSE, is the true SE, referring just to the error incurred by the interpolation and sampling processes.

Proof. The proof straightforwardly follows from Corollary 1 and eq. (31). \square

The above corollary indicates that the reconstruction performance depends on i) the estimation performance of $\{\hat{\zeta}_k^{\text{DL}}[n]\}_{n \in \mathcal{N}_{\text{tr}}}$, which is based on the choice of $\delta_{\text{tol}}^{\text{DL}}$, and ii) the performance of the interpolation process, which is measured by the TSE. In practice, the latter depends on the choice of the interpolation method (e.g., linear, cubic, spline [29]). We conclude that there is a clear trade-off between the duration of the training phase and the quality of the model \hat{f}_k : the smaller $\delta_{\text{tol}}^{\text{DL}}$, the longer the training phase duration ($\uparrow L_{\text{tr}}$), and the better would be the expected reconstruction performance as measured by $\overline{\text{SE}}$. On the other hand, keep in mind that a longer training duration means a higher overhead of the overall protocol and, hence, a lower throughput.

V. UPLINK ACCESS PHASE

In this section, we present the details of the UL access phase. First, we design an access configuration codebook, whose design goals are: i) to cover the area of interest, and ii) to ensure that the UL SNR is greater than a minimum threshold γ_{ac} regardless the position of the UEs so as to improve the probability that the AP successfully decodes their data packets. Second, we propose different access policies based on the inference step of the channel oracle. Third, we characterize the UL received signal at the AP.

A. Access Configuration Codebook

A straightforward design for the access codebook would be to uniformly slice the angular domain $\theta_r^{DL} \in [0, \pi/2]$ into N_{ac} slices. However, two problems occur when considering this design: there is no guarantee on the level of the UL received SNR of the UEs; the main lobe of the array factor in (9) has a width that depends on the reflection angle θ_r^{DL} [23], where the higher the value of θ_r^{DL} , the wider the main lobe. To solve these drawbacks, we introduce a tailored design for the access codebook Φ_{ac} together with a power control strategy that is carried out by the UEs. More formally, we want to design an access codebook and the UE's transmit power in order to have at least one configuration $n \in \mathcal{N}_{ac}$ that satisfies the following for UE $k \in \mathcal{K}$

$$\text{SNR}_k^{\text{UL}} \beta_k^{\text{UL}} |A_k(\theta_r^{\text{DL}}[n])|^2 > \gamma_{ac}, \quad (34)$$

where $\text{SNR}_k^{\text{UL}} = \frac{\rho_k}{\sigma^2}$ is the UL transmit SNR with ρ_k being the UL transmit power and σ^2 being the noise power at the AP. Observe that only $A_k(\theta_r^{\text{DL}}[n])$ is a function of the reflection angle θ_r^{DL} . The access codebook design is then divided into two steps: i) certify that $|A_k(\theta_r^{\text{DL}}[n])|^2$ gives a minimum gain and ii) make the UEs to adjust their transmit power ρ_k accordingly so as to meet the UL SNR threshold γ_{ac} .

Step 1. The normalized power contribution of the array factor can be rewritten as [23], [30]

$$\frac{|A_{b,k}(\theta_r^{\text{DL}}[n])|^2}{M^2} = \left| \frac{\sin\left(\frac{\omega d_x}{2} M_x (\sin \theta_k - \sin \theta_r^{\text{DL}}[n])\right)}{M_x \sin\left(\frac{\omega d_x}{2} (\sin \theta_k - \sin \theta_r^{\text{DL}}[n])\right)} \right|^2. \quad (35)$$

The above expression is the array factor of the linear phased array, a periodic function of the angular position having a main lobe of magnitude 1 (0 dB) centered in $\sin \theta_r^{\text{DL}}[n] = \sin \theta_k$ –which can be well approximated by the main lobe of a sinc function– and a side lobe level (SLL) value of approximately 0.045 (-13.46 dB) [23]. Thus, it is possible to design the access codebook

letting the main lobe of two consequent configurations to overlap at the angular point which provides the desired minimum gain, so that each UE can find at least one suitable configuration, regardless of its position. Let then $\tau \in (0.045, 1]$ be the minimum gain desired, where the lower limit is set to unambiguously discriminate the main lobe from the side lobes. We want to set x such that $|\text{sinc}(x)|^2 \geq \tau$. Defining $\pm x_\tau$ as the x that satisfy $|\text{sinc}(x_\tau)|^2 = \tau$, the condition is

$$-x_\tau < \pi F_0 M_x (\sin \theta_k - \sin \theta_r^{\text{DL}}[n]) < x_\tau,$$

where $F_0 = \frac{d_x}{\lambda}$ as in (13). Now, define as $\theta_r^{\text{DL},\tau^+}[n]$ and $\theta_r^{\text{DL},\tau^-}[n]$ the right and left angular directions where the gain of the main lobe is precisely τ , namely τ -angular directions. They can be obtained from the following relations

$$\pi F_0 M_x (\sin \theta_r^{\text{DL},\tau^+}[n] - \sin \theta_r^{\text{DL}}[n]) = x_\tau \text{ and } \pi F_0 M_x (\sin \theta_r^{\text{DL},\tau^-}[n] - \sin \theta_r^{\text{DL}}[n]) = -x_\tau. \quad (36)$$

To cover the whole area of interest (see Fig. 1), we impose that $\theta_r^{\text{DL},\tau^+}[N-1] = \pi/2$, meaning that the last configuration $n = N - 1$ has the left τ -angular direction towards the most left direction of the area of interest. Therefore, by using (36), we have

$$\sin \theta_r^{\text{DL}}[N-1] = 1 - \frac{x_\tau}{\pi F_0 M_x}.$$

By applying the above to compute $\theta_r^{\text{DL},\tau^-}[N-1]$, we obtain

$$\sin \theta_r^{\text{DL},\tau^-}[N-1] = 1 - 2 \frac{x_\tau}{\pi F_0 M_x} = \sin \theta_r^{\text{DL},\tau^+}[N-2],$$

which is then set to overlap the left τ -angular direction of configuration $N - 2$. By iterating the procedure, we get the following

$$\sin \theta_r^{\text{DL}}[n] = 1 - (2(N-n) - 1) \frac{x_\tau}{\pi F_0 M_x}, \forall n \in \mathcal{N}_{\text{ac}}. \quad (37)$$

Then, a lower bound on the number of access configurations needed to cover the whole area while incurring a minimum gain of τ is

$$N_{\text{ac}} \geq \min \{n \mid \sin \theta_r^{\text{DL},\tau^-}[n] < 0, n \in \mathbb{Z}_+\} = \left\lceil \pi \left(\frac{M_x}{2x_\tau} \right) F_0 \right\rceil. \quad (38)$$

Note the similarity with the lower bound obtained for the training codebook in eq. (25), with the additional factor x_τ which depends on the amount of power we allow to lose. The access configuration codebook $\Phi_{\text{ac}} \equiv \Theta_{\text{ac}}$ is then constructed based on the iterative method defined above given that N_{ac} is chosen according to the bound. Without loss of generality, we will consider $\tau = 0.5$ (-3 dB) based on classical literature, which gives $x_\tau \approx 1.391$ [23].

Step 2. Given an access codebook following the design of eqs. (37)-(38), there is at least one configuration, say n^* , providing an SNR of user k at the AP of

$$\frac{\rho_k}{\sigma^2} \beta_k^{\text{UL}} |A_k(\theta_r^{\text{DL}}[n^*])|^2 \geq \frac{\rho_k}{\sigma^2} \beta_k^{\text{UL}} M^2 \tau > \gamma_{\text{ac}}, \quad (39)$$

where the last inequality is imposed to meet the condition in (34). To satisfy the aforementioned condition, we devise a power control policy based on selecting the minimum UL transmit power at the UE's side. Since β_k^{UL} is a function of the random position of UE k , we assure the above inequality in the average sense with respect to the UE's position as follows³

$$\rho_k \geq \frac{\sigma^2}{\mathbb{E}_k\{\beta_k^{\text{UL}}\} M^2 \tau} \gamma_{\text{ac}}. \quad (40)$$

If we assume that d_k and θ_k are independent, the expectation evaluates to

$$\mathbb{E}_k\{\beta_k^{\text{UL}}\} = \frac{G_a G_k}{(4\pi)^2} \left(\frac{d_x d_z}{d_a}\right)^2 \mathbb{E}_k\left\{\frac{\cos^2 \theta_k}{d_k^2}\right\} = \frac{G_a G_k}{(4\pi)^2} \left(\frac{d_x d_z}{d_a}\right)^2 \frac{\log(d_{\max}) - \log(d_{\min})}{d_{\max}^2 - d_{\min}^2}, \quad (41)$$

with probability distribution functions (PDFs) given by

$$p_{d_k}(d) = \frac{2d}{(d_{\max}^2 - d_{\min}^2)}, \text{ for } d_{\min} \leq d \leq d_{\max}, \quad \text{and} \quad p_{\theta_k}(\theta) = \frac{2}{\pi}, \text{ for } 0 \leq \theta \leq \frac{\pi}{2}. \quad (42)$$

B. Access Policy

Each UE locally decides in which access slots to transmit its payload data by means of an access policy that can explore the model $\hat{f}_k : \theta_r^{\text{DL}} \mapsto \hat{\zeta}_k^{\text{DL}}$ obtained during the DL training phase. In principle, an access policy would like to satisfy two conditions: i) maximize the UL SNR received at the AP for each UE, *i.e.*, improve its probability of access, and ii) reduce the overall probability of collisions, *i.e.*, improve the system throughput. To satisfy the first condition, since the UL received SNR (34) is proportional to the UL channel response, a UE would like to transmit its payload data during the access slot associated to its best configuration or reflection angle $\theta_r^{\text{DL}}[n]$. To be able to find the best access slots in this sense, each UE performs the channel oracle inference step as:

$$\hat{\zeta}_k^{\text{UL}}[n] = \hat{f}_k(\theta_r^{\text{DL}}[n]), \forall n \in \mathcal{N}_{\text{ac}}, \quad (43)$$

where $\hat{\zeta}_k^{\text{UL}}[n] \in \mathbb{C}$ is the inferred UL channel response for the n -th access slot at the UE's side. Let $\hat{\zeta}_k^{\text{DL}} \in \mathbb{C}^{\mathcal{N}_{\text{ac}}}$ denote the collection of inferences from (43). Thus, the UE can exploit $\hat{\zeta}_k^{\text{DL}}$

³For the sake of analysis, we keep the power of all UEs the same. Nevertheless, each UE could use an estimation of the largest UL channel responses to derive a power control policy or different statistics other than average.

so as to choose to transmit during the access slots that provides him good UL received SNRs. To satisfy the second condition, we assume that the UEs cannot coordinate among themselves. Then, we consider that the best a UE can do to avoid collisions is to transmit multiple replicas of its packet inspired by the regular repetition slotted ALOHA [25].

We now formally define an access policy. Let $\Pi_k \subseteq \mathcal{N}_{\text{ac}}$ denote the access set that contains the access slots in which the k -th UE will actually attempt to send its packet, where $|\Pi_k| = R$, $R \in \mathbb{Z}_+$, defines the number of replicas to send. To obtain its Π_k , a UE first quantifies the relevance of the access slots based on an *acquisition function* $q : \mathbb{C} \mapsto \mathbb{R}$ that uses the element of the inferred information $\hat{\zeta}_k^{\text{DL}}$ as an input. With the measured qualities of the access slots in hand, the UE applies a *selection function* $s : \mathbb{R} \mapsto \mathcal{N}_{\text{ac}}$, which actually defines how to build the access set. By making a parallel to the reinforcement learning literature [31], the acquisition function can be learned or specified, while the selection function can be deterministic or stochastic. For simplicity, we consider a heuristically defined acquisition function as $q = |\cdot|$ in the access policies introduced below.

1) *R-configuration-aware random policy (R-CARAP)*: The UE can compute a probability mass function $\mathbf{p} \in \mathbb{R}^{\mathcal{N}_{\text{ac}}}$ where the n -th element of \mathbf{p} is given as

$$P_n = \frac{q(\hat{\zeta}_k^{\text{UL}}[n])}{\sum_{n'=1}^{\mathcal{N}_{\text{ac}}} q(\hat{\zeta}_k^{\text{UL}}[n'])}. \quad (44)$$

The selection function is then a random function comprised of sampling without replacement the elements from the set \mathcal{N}_{ac} based on \mathbf{p} and R . The construction of Π_k finalizes when the specified R is reached.

2) *R-greedy-strongest-configurations access policy (R-GSCAP)*: See Algorithm 1.

Algorithm 1: R-GSCAP

Data: \mathcal{N}_{ac} , R , $q = |\cdot|$, $\Pi_k = \emptyset$

Result: Π_k

```

1 while  $|\Pi_k| \leq R$  do
2    $n^* = \arg \max_{n \in \mathcal{N}_{\text{ac}}} q(\hat{\zeta}_k^{\text{UL}}[n])$  # selection function;
3    $\Pi_k = \Pi_k \cup \{n^*\}$ ;
4    $\mathcal{N}_{\text{ac}} = \mathcal{N}_{\text{ac}} \setminus \{n^*\}$ 

```

3) *Strongest-minimum access policy (SMAP)*: Different from the others, this is the only policy that is not defined for any number of multiple replicas. SMAP simply follows from a heuristic of

transmitting only two replicas, $R = 2$, according to the following. The first replica is transmitted during the best access slot, that is, $n_1 = \arg \max_{n \in \mathcal{N}_{\text{ac}}} q(\hat{\zeta}_k^{\text{UL}}[n])$. Whereas the second replica is transmitted into the access slot that is closest to ensure the UL minimum SNR threshold γ_{ac} , which can be written as

$$n_2 = \arg \min_{n \in \mathcal{N}_{\text{ac}} \setminus \{n_1\}} \left\{ \text{SNR}_k^{\text{UL}} |\hat{\zeta}_k^{\text{UL}}[n]|^2 - \gamma_{\text{ac}} \mid \text{SNR}_k^{\text{UL}} |\hat{\zeta}_k^{\text{UL}}[n]|^2 \geq \gamma_{\text{ac}} \right\} \quad (45)$$

Then, $\Pi_k = \{n_1, n_2\}$. If n_2 does not exist, the UE transmits just in slot n_1 .

C. Uplink Received Access Signal

The AP controls the RIS to sweep over the access codebook Φ_{ac} , establishing the corresponding access slots. Meanwhile, the UEs transmit their payload data following their access set Π_k . Let $\mathcal{K}_n \subseteq \mathcal{K}$ denote the subset of contending UEs having chosen to transmit in the n -th access slot, *i.e.*, $\mathcal{K}_n = \{k : n \in \Pi_k, \forall k \in \mathcal{K}\}$, $n \in \mathcal{N}_{\text{ac}}$. The received signal $\mathbf{v}[n] \in \mathbb{C}^{L_{\text{ac}}}$ at the AP is

$$\mathbf{v}[n] = \sqrt{\rho_k} \sum_{k \in \mathcal{K}_n} \zeta_{a,k}^{\text{UL}}[n] \boldsymbol{\nu}_k + \boldsymbol{\eta}_a[n], \quad (46)$$

where $\boldsymbol{\nu}_k \in \mathbb{C}^{L_{\text{ac}}}$ is the packet of the k -th UE with zero mean and $\mathbb{E}\{\|\boldsymbol{\nu}_k\|_2^2\} = L_{\text{ac}}$, and $\boldsymbol{\eta}_b[n] \in \mathbb{C}^{L_{\text{ac}}} \sim \mathcal{N}_{\mathbb{C}}(\mathbf{0}, \sigma^2 \mathbf{I}_{L_{\text{ac}}})$ is the receiver noise at the AP. Again, noise samples are i.i.d. over n . We note that L_{ac} corresponds to the number of symbols that comprises the packets of the k -th UE. The AP runs a decoding process over $\{\mathbf{v}[n]\}_{n \in \mathcal{N}_{\text{ac}}}$ that uses a collision resolution strategy as detailed in [19, Algo. 1]. After the decoding is complete, the AP holds the set of successfully decoded UEs as $\mathcal{K}_{\text{ac}} \subseteq \mathcal{K}$ with $|\mathcal{K}_{\text{ac}}| = K_{\text{ac}}$ and a corresponding list of access slots in which each member of \mathcal{K}_{ac} was successfully decoded, denoted as $\mathcal{N}_{\text{ac}}^{\text{dec}} \subseteq \mathcal{N}_{\text{ac}}$, $|\mathcal{N}_{\text{ac}}^{\text{dec}}| \leq K_{\text{ac}}$. Note that we can define the following non-injective surjective mapping between those sets

$$\mu : \mathcal{K}_{\text{ac}} \mapsto \mathcal{N}_{\text{ac}}^{\text{dec}}. \quad (47)$$

VI. DOWNLINK ACKNOWLEDGMENT PHASE

Here, we propose how the RIS can assist the ACK process, introducing two ways to design the ACK configuration codebook, and characterizing the signal received by the UEs.

A. Acknowledgment Configuration Codebook

The AP designs a third configuration codebook to send the ACK messages based on the successfully decoded UEs in \mathcal{K}_{ac} at a given RA frame, whose goal is to increase the probability that the UEs in \mathcal{K}_{ac} will be correctly informed that their messages were decoded by the AP. Below, we devise two heuristic approaches for such.

1) *Precoding-based acknowledgment*: Based on the maximum-ratio precoding [32], we consider a codebook that has a single configuration:

$$\Phi_{\text{ack}} = \left\{ h^{-1} \left(\frac{1}{K} \sum_{n \in \mathcal{N}_{\text{ac}}^{\text{dec}}} \theta_r^{\text{DL}}[n] \right) \right\}, \quad (48)$$

where we use the definition of h in (7). In fact, by the law of large numbers, $\theta_r^{\text{DL}} \rightarrow \frac{\pi}{4}$. The advantage of using a single configuration is the reduction of the impact of the switching time T_{sw} in (10). The price to pay for this reduced impact is an expected reduced probability of successful ACK since the average configuration can bring low SNR conditions to some UEs.

2) *TDMA-based acknowledgment*: Based on channel reciprocity, another approach is

$$\Theta_{\text{ack}} = \{\theta_r^{\text{DL}}[n] : n \in \mathcal{N}_{\text{ac}}^{\text{dec}}\}, \text{ and } \Phi_{\text{ack}} = h^{-1}(\Theta_{\text{ack}}), \quad (49)$$

that is, we use the configurations associated with the access slots that led to successfully decoded UEs with $|\Theta_{\text{ack}}| \leq K_{\text{ac}}$. Clearly, we now have the opposite trade-off: The ACK phase takes longer because of the increased switching time, whereas the probability of UEs successfully getting their ACK messages is increased due to improved DL received SNRs.

B. Downlink Received Acknowledgment Signal

The AP sends ACK messages towards the UEs with the help of the RIS, whereas the UEs try to decode them. Thus, for $k \in \mathcal{K}_{\text{ac}}$, the k -th UE receives $\mathbf{w}'_k[k] \in \mathbb{C}^{L_{\text{ack}}}$ at the k -th ACK slot:

$$\mathbf{w}'_k[k] = \sqrt{\rho_a} \zeta_k^{\text{DL}}[\mu(k)] \alpha_k + \eta'_k[k], \quad (50)$$

where $\alpha_k \in \mathbb{C}^{L_{\text{ack}}}$ is the ACK message meant to the k -th UE. The channel response $\zeta_k^{\text{DL}}[\mu(k)]$ is with respect to the configuration $\theta_r^{\text{DL}}[n] \in \Theta_{\text{ack}}$, where n is chosen from $\mathcal{N}_{\text{ac}}^{\text{dec}}$ according to UE $k \in \mathcal{K}_{\text{ac}}$ following the definition of μ in (47). Thus, the set of successfully decoded UEs that successfully received their ACKs is

$$\mathcal{K}_{\text{ack}}^i = \left\{ k : \frac{\|\mathbf{w}'_k[k]\|_2^2}{L_{\text{ack}} \sigma^2} \geq \gamma_{\text{ack}}, k \in \mathcal{K}_{\text{ac}} \right\} \text{ with } \mathcal{K}_{\text{ack}}^i \subseteq \mathcal{K}_{\text{ac}}, \quad (51)$$

where $i \in \{\text{'prec'}, \text{'tdma'}\}$ depending on the choice of the ACK configuration codebook. Thus, the UEs in $\mathcal{K}_{\text{ack}}^i$ end their access attempts, while the set of unsuccessful UEs is $\mathcal{K}_{\text{uc}}^i = \mathcal{K} \setminus \mathcal{K}_{\text{ack}}^i$.

VII. NUMERICAL RESULTS

In this section, we evaluate the proposed RA protocol going through each designed step. Table I summarizes the standard simulation parameters used. The DL received SNR ranges from approximately -122 to 32 dB, while -132 to 22 dB is the range for the UL received SNR. As a reference point, we focus on the case where the UEs send a single packet $R = 1$ with the exception of the SMAP, where $R \leq 2$. To evaluate the RA performance, we introduce two metrics. First, the expected probability of access is

$$\bar{P}_{\text{ac}}^j = \mathbb{E}\{\Pr\{k \in \mathcal{A}_j | \forall k \in \mathcal{K}\}\}, \quad (52)$$

where $j \in \{\text{'ac'}, \text{'prec'}, \text{'tdma'}\}$ with $\mathcal{A}_j \in \{\mathcal{K}_{\text{ac}}, \mathcal{K}_{\text{ack}}^{\text{prec}}, \mathcal{K}_{\text{ack}}^{\text{tdma}}\}$. The expectation is taken with respect to noise realizations and the realization of different collision setups given a fixed channel load κ . Moreover, j indexes in which moment of the RA protocol the expected probability of access is evaluated. Second, we introduce the expected throughput as

$$\bar{\text{th}}^j = \mathbb{E}\left\{\frac{|\mathcal{A}_j|}{T}\right\} = \mathbb{E}\left\{\frac{|\mathcal{A}_j|}{T_{\text{tr}} + T_{\text{ac}} + T_{\text{ack}}}\right\} \text{ [packet/channel use]}, \quad (53)$$

where the expectation and the meanings of j and \mathcal{A}_j are as before. The definitions of the terms in the denominator follow eq. (10). On one hand, when $j = \text{'prec'}$ and $j = \text{'tdma'}$, the accessed probability of access and the throughput are end-to-end. On the other hand, when $j = \text{'ac'}$, just evaluates the UL direction of those with $T_{\text{ack}} = 0$. Essentially, both metrics are highly dependent on the choice of the access policies Π_k , parameter values, such as the threshold SNRs $\gamma_{\text{ac}}, \gamma_{\text{ack}}$, and the decoding method employed at the AP. However, we omit the indexation of such dependencies for the sake of clarity. In the following results, we calculate the above expectations numerically by using Monte Carlo simulations.

Regular Repetition Slotted ALOHA (RRS-ALOHA). As a baseline, we consider the regular repetition slotted ALOHA, where regular and repetition mean that all UE can repeat its packet by the same amount of R times. In this particular case, the UEs do not exploit channel oracle and select the slots uniformly at random without replacement. Consequently, the training phase is ignored and the expected end-to-end throughput is calculated as $\bar{\text{th}}^j = \mathbb{E}\{\mathcal{A}_j / (T_{\text{ac}} + T_{\text{ack}})\}$.

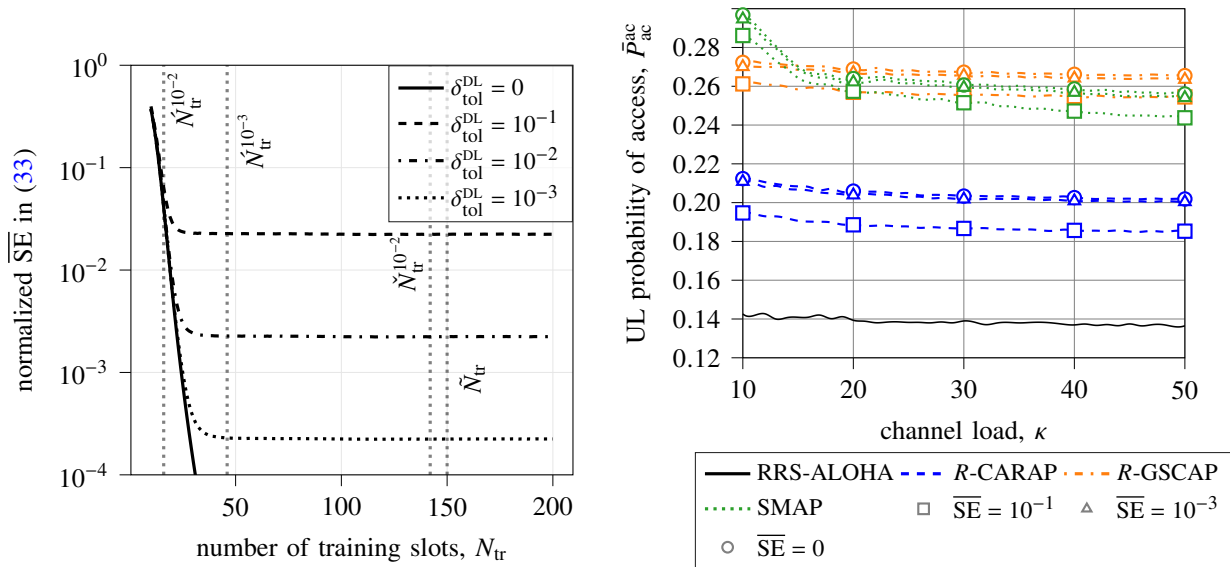
We start by evaluating how efficient is the DL training phase in providing a good model $\hat{f}_k : \theta_r^{\text{DL}} \mapsto \hat{\zeta}_k^{\text{DL}}$. Figure 5a shows the normalized expected SE of the model, specified in Corollary 2. In

TABLE I
SIMULATION PARAMETERS

Parameter	Value	Parameter	Value
carrier frequency, f_c	3 GHz	antenna gains, G_a, G_k	5 dB
# elements along axes, M_x, M_z	10	AP transmit power, ρ_a	20 dBm
element sizes, d_x, d_z	λ	UE transmit power ρ_k	10 dBm
max. and min distances, d_{\max}, d_{\min}	100, 5 m	threshold decoding SNR, $\gamma_{ac}, \gamma_{ack}$	3 dB
AP-RIS distance, d_a	d_{\min}	# of symbols, L_{ac}, L_{ack}	1
AP-RIS angle, θ_a	45°	# of repetitions R	1

particular, we used the spline interpolating function and considered different estimation tolerances $\delta_{\text{tol}}^{\text{DL}}$, defined in Corollary 1. The figure evaluates the design of the training configuration codebook carried out in Subsection IV-A by drawing some of the approximated lower bounds obtained below eq. (26). We verify that the reconstruction error is dominated by noise and estimation effects parameterized by $\delta_{\text{tol}}^{\text{DL}}$, as expected from the result of Corollary 2. For the most conservative bound of $\hat{N}_{\text{tr}}^{10^{-2}} = 16$ (median w/ $\epsilon = 10^{-2}$), the expected SE is considerably high – on the order of 10^{-1} , showing that this bound fairly undersamples the function we are interested in reconstructing. On the other hand, $\check{N}_{\text{tr}}^{10^{-2}} = 142$ (maximum w/ $\epsilon = 10^{-2}$), and $\tilde{N}_{\text{tr}} = 150$ (Taylor-approximation) oversample the function since they ensure the same quality that $\hat{N}_{\text{tr}}^{10^{-3}} = 46$ (median w/ $\epsilon = 10^{-3}$) does. Thus, we chose the approximated bound $\hat{N}_{\text{tr}}^{10^{-3}} = 46$ configurations because it minimizes the size of the training phase and allows us to reach a wide range of possible reconstruction errors.

To further support the choice of $\hat{N}_{\text{tr}}^{10^{-3}} = 46$, we evaluate the impact of the normalized expected SE of the reconstruction in (33) on the expected probability of access in Fig. 5b. In particular, we assumed that the size of the access slot N_{ac} is equal to the channel load κ based on the optimal throughput analysis of the classic slotted ALOHA protocol [25], while ensuring the lower bound in (38). We can see that the reconstruction error affects the performance of the channel-oracle-based access policies. However, the curves with a $\overline{\text{SE}} = 10^{-3}$ almost reach the perfect-reconstruction ones with $\overline{\text{SE}} = 0$, showing that the performance loss is almost negligible when $\overline{\text{SE}} = 10^{-3}$. Observe that the lower bound $\hat{N}_{\text{tr}}^{10^{-3}} = 46$ enables us to achieve the reconstruction error of $\overline{\text{SE}} = 10^{-3}$. Based on the obtained results, we parameterize the reconstruction error to be $\overline{\text{SE}} = 10^{-3}$ and set L_{tr} according to Corollary 1 for the following simulations.



(a) Normalized expected squared error (SE) of the reconstructed model $\hat{f}_k : \theta_r^{DL} \mapsto \hat{\zeta}_k^{DL}$ when using spline interpolation function. Noiseless reconstruction happens when $\delta_{tol}^{DL} = 0$. (b) UL Expected probability of access w/o ACK $T_{ack} = 0$ for $N_{ac} = \kappa$. Perfect reconstruction is obtained when $\overline{SE} = 0$.

Fig. 5. Evaluation of the DL training phase. In Fig. 5a, the approximated lower bounds below eq. (26) were plotted according to: $\hat{N}_{tr}^{10^{-2}} = 16$ (median w/ $\epsilon = 10^{-2}$), $\hat{N}_{tr}^{10^{-3}} = 46$ (median w/ $\epsilon = 10^{-3}$), $\check{N}_{tr}^{10^{-2}} = 142$ (maximum w/ $\epsilon = 10^{-2}$), and $\tilde{N}_{tr} = 150$ configurations (Taylor-approximation).

Figure 6 shows the average throughput when considering different stages of the RA protocol, both ACK methods, and the different proposed access policies. The switching time is set to zero $T_{sw} = 0$ in order to neglect the effect of RIS hardware in this analysis. From the figure, we observe the following. When channel load κ is low, a worse performance is obtained by the access policies that make use of the channel oracle. This is caused by the fact that the size of the DL training phase, $N_{tr} = \hat{N}_{tr}^{10^{-3}} = 46$, is larger than the UL access phase, $N_{ac} = \kappa$. However, after the channel load κ becomes comparable in size to $\hat{N}_{tr}^{10^{-3}}$, there is a great advantage in using the access policies based on channel oracle. Interestingly, the RRS-ALOHA baseline reaches a performance floor, while the other methods keep increasing. What is noteworthy is that the evaluated scenario benefits the RRS-ALOHA since $N_{ac} = \kappa$ [25], which results in the theoretical optimal throughput for such access policy. Thus, the obtained results greatly highlight the gains brought by the channel oracle enabled by the RIS. For the channel-oracle-based policies, it is expected that more gains can be obtained by optimizing the value of N_{ac} . Of course, there is a trade-off in optimizing N_{ac} that needs further study, as the RA frame can take longer.

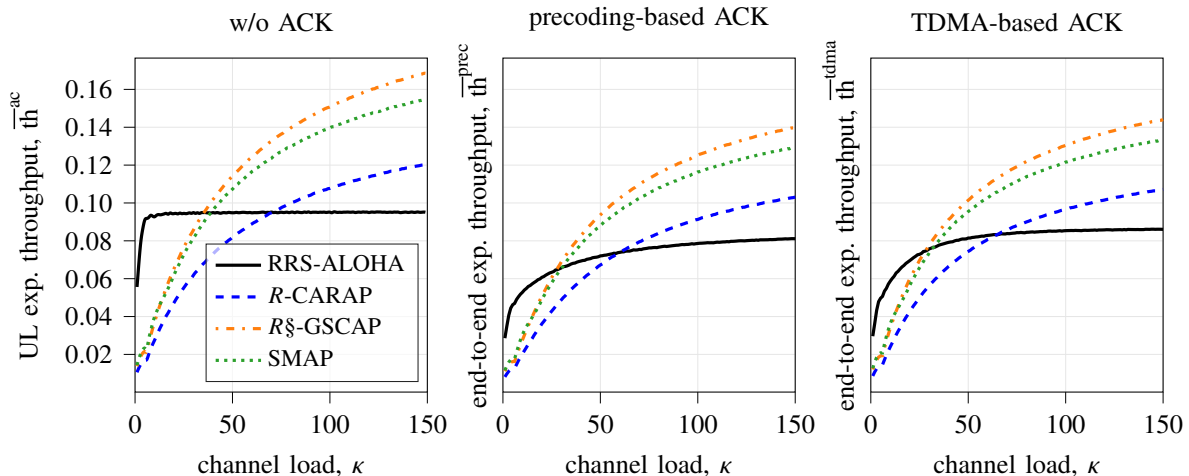


Fig. 6. Expected system throughput vs channel load when assuming that $N_{ac} = \kappa$ and such that N_{ac} always respect the bound in (38). For reference, the switching time is set to zero, $T_{sw} = 0$.

From Fig. 6, we also observe that the *R-GSCAP* outperforms the other channel-oracle-based access policies. Moreover, it is evident that ACK impacts negatively the throughput. There is a slight tendency of getting better results with the TDMA-based ACK, since $T_{sw} = 0$ and the precoding-based favors UEs located around $\theta_k = 45^\circ$.

Focusing on the best channel-oracle-based access policy *R-GSCAP* and the proposed ACK methods, we end our analysis by showing the impact of the RIS hardware/communication by varying the switching time T_{sw} in Fig. 7. Based on 5G-NR and LTE systems, the duration of a time slot is around 1 ms. Thus, we set $T = 1$ to correspond to a delay of 0.5 ms, while $T = 5$ of 2.5 ms. Therefore, we note that the protocol is very sensitive to hardware or communication latency. There is an evident need for careful design of the RIS and the CC between the AP and the RIS so that the protocol operates at close to its best capacity. However, in view of recent works [33], the RIS switching time is on the order of the μs , making the protocol feasible to be implemented in practice with good performance efficiency.

VIII. CONCLUSION

To the best of our knowledge, this paper proposes the first RA protocol that carefully integrates the RIS into its design considering the scenario of interest in Fig. 1. Our protocol numerically outperforms the RRS-ALOHA by 40% on average in terms of the end-to-end throughput, showing that there is room for a new class of protocols that explicitly consider the new aspects of environmental control brought about by RIS. In particular, we hope that our work will inspire

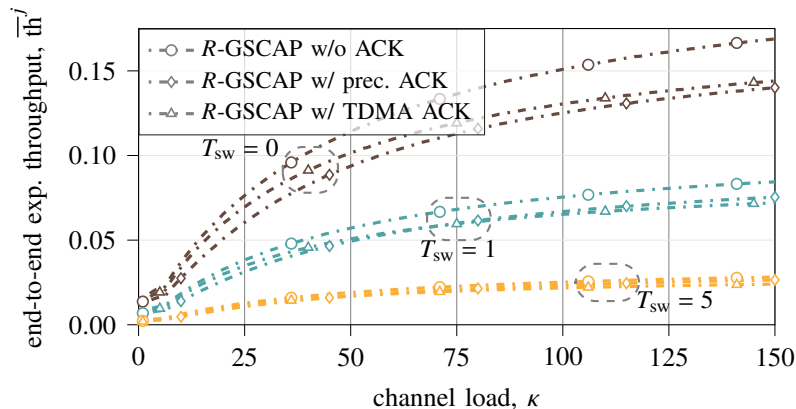


Fig. 7. Evaluation of the hardware and communication latency introduced by the RIS on the proposed protocol when using the best access policy, R -GSCAP. The corresponding times are 0.5 ms for $T_{sw} = 1$ and 2.5 ms for $T_{sw} = 5$.

further optimization and theoretical analysis of our protocol and the emergence of new protocols that properly integrate the RIS.

ACKNOWLEDGMENT

This work was supported by the Villum Investigator Grant “WATER” from the Velux Foundation, Denmark, and the H2020 RISE-6G project.

REFERENCES

- [1] C. Huang, A. Zappone *et al.*, “Reconfigurable intelligent surfaces for energy efficiency in wireless communication,” *IEEE Transactions on Wireless Communications*, vol. 18, no. 8, pp. 4157–4170, 2019.
- [2] E. C. Strinati, G. C. Alexandropoulos *et al.*, “Wireless environment as a service enabled by reconfigurable intelligent surfaces: The RISE-6G perspective,” in *Proc. Joint European Conference on Networks and Communications 6G Summit (EuCNC/6G Summit)*, 2021, pp. 562–567.
- [3] A. Pizzo, L. Sanguinetti, and T. L. Marzetta, “Spatial characterization of electromagnetic random channels,” *IEEE Open Journal of the Communications Society*, vol. 3, pp. 847–866, 2022.
- [4] —, “Fourier plane-wave series expansion for holographic MIMO communications,” *IEEE Transactions on Wireless Communications*, vol. 21, no. 9, pp. 6890–6905, 2022.
- [5] E. Björnson, H. Wymeersch *et al.*, “Reconfigurable intelligent surfaces: A signal processing perspective with wireless applications,” *IEEE Signal Processing Magazine*, vol. 39, no. 2, pp. 135–158, 2022.
- [6] C. Ross, G. Gradoni *et al.*, “Engineering reflective metasurfaces with ising hamiltonian and quantum annealing,” *IEEE Transactions on Antennas and Propagation*, vol. 70, no. 4, pp. 2841–2854, 2021.
- [7] V. Jamali, G. C. Alexandropoulos *et al.*, “Low-to-zero-overhead IRS reconfiguration: Decoupling illumination and channel estimation,” *IEEE Communications Letters*, vol. 26, no. 4, pp. 932–936, 2022.
- [8] P. Mursia, V. Sciancalepore *et al.*, “RISMA: Reconfigurable intelligent surfaces enabling beamforming for IoT massive access,” *IEEE Journal on Selected Areas in Communications*, vol. 39, no. 4, pp. 1072–1085, 2020.

- [9] X. Wei, D. Shen, and L. Dai, "Channel estimation for RIS assisted wireless communications — Part I: Fundamentals, solutions, and future opportunities," *IEEE Communications Letters*, vol. 25, no. 5, pp. 1398–1402, 2021.
- [10] J. Yuan, G. C. Alexandropoulos *et al.*, "Tensor-based channel tracking for RIS-empowered multi-user MIMO wireless systems," *arXiv preprint arXiv:2202.08315*, 2022.
- [11] J. Yuan, E. De Carvalho *et al.*, "Frequency-mixing intelligent reflecting surfaces for nonlinear wireless propagation," *IEEE Wireless Communications Letters*, vol. 10, no. 8, pp. 1672–1676, 2021.
- [12] P. Wang, J. Fang *et al.*, "Compressed channel estimation for intelligent reflecting surface-assisted millimeter wave systems," *IEEE signal processing letters*, vol. 27, pp. 905–909, 2020.
- [13] Y. Polyanskiy, "A perspective on massive random-access," in *2017 IEEE International Symposium on Information Theory (ISIT)*, 2017, pp. 2523–2527.
- [14] A.-S. Bana, E. de Carvalho *et al.*, "Massive MIMO for internet of things (IoT) connectivity," *Physical Communication*, vol. 37, p. 100859, 2019.
- [15] X. Cao, B. Yang *et al.*, "Massive access of static and mobile users via reconfigurable intelligent surfaces: Protocol design and performance analysis," *IEEE Journal on Selected Areas in Communications*, pp. 1–1, 2022.
- [16] X. Shao, L. Cheng *et al.*, "A Bayesian tensor approach to enable RIS for 6G massive unsourced random access," in *Proc. IEEE Global Communications Conference (GLOBECOM)*, 2021.
- [17] F. Laue, V. Jamali, and R. Schober, "RIS assisted device activity detection with statistical channel state information," 2022.
- [18] A. A. Kherani and S. T. V., "On RIS-assisted random access systems with successive interference cancellation," in *2022 National Conference on Communications (NCC)*, 2022, pp. 13–17.
- [19] V. Croisfelt, F. Saggese *et al.*, "A random access protocol for RIS-aided wireless communications," in *2022 IEEE 23rd International Workshop on Signal Processing Advances in Wireless Communication (SPAWC)*, 2022, pp. 1–5.
- [20] A. Munari, M. Heindlmaier *et al.*, "The throughput of slotted ALOHA with diversity," in *2013 51st Annual Allerton Conference on Communication, Control, and Computing (Allerton)*, 2013, pp. 698–706.
- [21] C. A. Balanis, *Advance engineering electromagnetics*, 2nd ed. Wiley, 2012.
- [22] J. G. Proakis and D. K. Manolakis, *Digital Signal Processing (4th Edition)*, 4th ed. Prentice Hall, 2006.
- [23] C. A. Balanis, *Antenna theory: analysis and design*. Wiley-Interscience, 2005.
- [24] O. Özdoğan, E. Björnson, and E. G. Larsson, "Intelligent reflecting surfaces: Physics, propagation, and pathloss modeling," *IEEE Wireless Communications Letters*, vol. 9, no. 5, pp. 581–585, 2020.
- [25] P. Popovski, *Wireless Connectivity: An Intuitive and Fundamental Guide*. Wiley, May 2020.
- [26] Y. Eldar, *Sampling Theory: Beyond Bandlimited Systems*. Cambridge University Press, 2015.
- [27] A. Pizzo, A. d. J. Torres *et al.*, "Nyquist sampling and degrees of freedom of electromagnetic fields," *IEEE Transactions on Signal Processing*, vol. 70, pp. 3935–3947, 2022.
- [28] S. M. Kay, *Fundamentals of Statistical Signal Processing: Estimation Theory*. Prentice Hall, 1997.
- [29] R. W. Hamming, *Numerical Methods for Scientists and Engineers (2nd Ed.)*. USA: Dover Publications, Inc., 1986.
- [30] W. Tang, M. Z. Chen *et al.*, "Wireless communications with reconfigurable intelligent surface: Path loss modeling and experimental measurement," *IEEE Transactions on Wireless Communications*, vol. 20, no. 1, pp. 421–439, 2020.
- [31] C. M. Bishop, *Pattern Recognition and Machine Learning*. Springer, 2006.
- [32] E. Björnson, J. Hoydis, and L. Sanguinetti, "Massive MIMO networks: Spectral, energy, and hardware efficiency," *Foundations and Trends® in Signal Processing*, vol. 11, no. 3-4, pp. 154–655, 2017.
- [33] V. Popov, M. Odit *et al.*, "Experimental demonstration of a mmWave passive access point extender based on a binary reconfigurable intelligent surface," 2021.